Paper No.
9319

NACE INTERNATIONAL CORROSION 2017 Conference & Expo

Electrochemistry of Mackinawite Electrodes in Sour Aqueous Solutions

M. Tjelta and J. Kvarekvål
Institute for Energy Technology (IFE)
Instituttveien 18
NO-2007, Kjeller, Norway

ABSTRACT

Iron sulfide, frequently found on carbon steel exposed to sour conditions, is under certain conditions expected to act as a (large area) cathode thereby increasing the corrosion rate of the underlying steel through galvanic coupling. In this work electrochemical reactions taking place at mackinawite (the most common low temperature polymorph of iron sulfide) electrodes in sour aqueous solutions have been studied using electrochemical techniques and the effect of mass transport was obtained using a jet impingement setup. The main objective was to obtain current-potential relations for iron sulfides which can be taken into a modelling framework, thereby allowing the estimation of the galvanic coupling between carbon steel and iron sulfides under different environmental conditions. In order to do so a method to produce mackinawite electrodes was developed. Part of this paper is therefore devoted to describing the FeS manufacturing process and to some physical characteristics to the produced mackinawite and the electrode itself.

Key words: Sour corrosion, mackinawite, H_2S, iron sulfide electrochemistry

INTRODUCTION

Iron sulfides in various polymorphs may form on steel surfaces under sour conditions. The layer formed can be either protective or increase the corrosion rate of the underlying steel, depending on conditions. Sour corrosion can therefore be a big problem in pipelines connected to reservoirs containing H_2S. Even though alloys resistant to both CO_2 and H_2S exist, the use of carbon steel is still attractive and widely used due to its lower cost.[1]

A significant body of work has been done on the corrosion of steel under various sour conditions. Models, also including the effect of multiphase flow [2], have been demonstrated to give good prediction on general corrosion rates.[3] When it comes to localized corrosion the understanding is more limited, but some factors promoting localized corrosion have been identified. Studies of corrosion under deposits (under-deposit corrosion, UDC) of iron sulfide

indicate increased corrosion rates and susceptibility to localized attack.[4,5] When in contact with steel, iron sulfide is expected to act as a cathode thereby increasing the corrosion rate of the underlying steel through galvanic coupling. If we imagine a situation with an iron sulfide film which has partly lost its protective ability due to some film flaw (typically cracking or delamination) with a layer of porous deposits on top, the cathode to anode ratio can become very large and the outcome may be severe localized corrosion. According to reference [4], mackinawite deposits result in significantly increased corrosion rates, while troilite/pyrrhotite deposits do not. However, in-house (unpublished) experiments indicate that under deposit corrosion is significant also under troilite/pyrrhotite.

In order to understand, and ultimately model, the effect iron sulfide films and deposits has for the corrosion rate on the underlying steel, more knowledge about the electrochemical behavior iron sulfides is needed. While a lot of effort has been put into understanding the chemical [6] and thermodynamic [7] properties of iron sulfides there are few studies on their electrochemical properties.[8]

Mackinawite is a polymorph of iron sulfide and the first one to form in sour corrosion. It is a metastable compound, but in-house experience indicates that it remains the dominating phase for prolonged periods of time, as long as the temperature is kept below a certain limit. The range of stability for mackinawite appears to depend on several parameters in addition to temperature, such as the partial pressure of H_2S and pH. Mackinawite has been shown to transform into greigite (Fe_3S_4) in anoxic water (i.e. without dissolved O_2 or excess S^{2-}), at least at low pH (typically around 3), and the conversion is reported to be quite fast above 70 °C.[6] In a study at 90 °C using conditions corresponding to roughly 0.3 bar H_2S, mackinawite was reported as the only corrosion product. Pyrrhotite, an iron sulfide polymorph thermodynamically stabile with respect to mackinawite, was found as the dominating corrosion product after exposure to 15 bar H_2S at 60 °C.[9] In the same study, mackinawite was found as the dominating product between 1.5 and 10 bar H_2S. Several other examples of conditions where the different iron sulfide polymorphs form are given in the review by Smith and Joosten[10], the general trend being that increasing temperature, time and H_2S partial pressure favor the formation of pyrrhotite (at the expense of mackinawite).

Mackinawite, in general, thus appears to be the most important low-temperature polymorph in sour corrosion. Troilite, pyrrhotite and pyrite (which are all commercially available materials) electrodes have been studied earlier [8,11,12] but is still work in progress. The objective of this work is to investigate the reactions taking place at mackinawite electrodes in sour aqueous systems to elucidate in particular the possible cathodic reactions. In order to do so a method to produce mackinawite electrodes was developed. To the best of our knowledge this is the first report of the use of mackinawite electrodes. Part of this paper is therefore devoted to describe the process of manufacture and to some physical characteristics to the electrode itself.

EXPERIMENTAL

Mackinawite synthesis

Steel shavings, cut from X65 pipeline steel, were reacted with dissolved H_2S at a partial pressure of 10 bars in a sealed autoclave at room temperature (~25°C). The aqueous solution contained 0.5 M NaCl and 1.23 M HCl to give a starting pH calculated to be 3. Care was taken

to remove dissolved oxygen by purging the solution with N_2 before introducing it to the autoclave.

After the reaction had been allowed to react for 42 days the corrosion product was immediately transferred to a glove box with a nitrogen atmosphere. Here the product was separated from the remaining shavings by repeated dispersion in isopropanol, centrifugation and decantation. Finally, the product was allowed to dry in the nitrogen atmosphere before being mortared.

X-ray diffractograms were recorded with Bruker Advance[†] with Cu-K radiation using a step size of 0.02° and a speed of 12 seconds per step. Specimens were prepared by spreading powders dispersed in acetone on a Si-crystal sample holder. The solvent was then allowed to evaporate, leaving behind a thin layer of sample. Note that the XRD-sample was kept in a dome-shaped air tight holder filled with nitrogen whilst recording diffractograms. Actually, this very same sample was re-examined at uneven intervals after up to 391 days of storage in a glove box.

Electrode fabrication

Mortared mackinawite powders from the synthesis described above were loaded into a pressing tool with a diameter of 6 mm. A uniaxial load of 3.5 tons allowed the fabrication of mechanically stable pellets without the use of a binder.

Electrical connections were attached to the mackinawite pellets using silver paste, and the electrodes were then casted in epoxy. Before each experiment a fresh electrode surface was obtained by grinding with SiC paper and polished to a mirror finish using 0.05 µm alumina. Note that the electrodes were somewhat porous, so the actual surface area was larger than the geometric one used to obtain area normalized quantities (e.g. current density).

Electrochemical measurements

All electrochemical measurements were performed using a conventional three-electrode setup in sealed glass cells. For potentiodynamic sweeps and for electrochemical impedance spectroscopy (EIS) the counter electrode was a coil of platinum wire with a total surface area of approximately 4 cm^2. The reference electrode was Ag/AgCl and potentials are referred to this, unless stated otherwise.

The base electrolyte was 0.5 M NaCl (~3 wt. %) in all experiments and the solution was purged with nitrogen overnight to remove dissolved oxygen. In order to avoid introduction of oxygen, the glass cell was assembled and sealed with all electrodes connected using Swagelok[†] fittings before being flushed with nitrogen. The pre-purged electrolyte was the introduced directly from a tank pressurized with nitrogen. H_2S was introduced by constant purging, thus maintaining a total pressure close to 1 atm. Partial pressures lower than 1 atm (minus vapor pressure) was obtained by mixing H_2S with N_2 in the desired ratio using mass flow controllers Adjustments of pH were done using NaOH or HCl. A summary of the experimental conditions is given in Table 1.

[†] Trade name

Electrochemical experiments were performed using either Gamry Ref 600‡ or Interface 1000 potentiostat. Polarization curves were recorded using a sweep rate of 0.1 $mV \cdot s^{-1}$, typically in a range of -500 mV away from the open circuit potential. A typical series of experiments was conducted in the following way: The relevant gas mixture was introduced to the system and equilibrium between gas and dissolved acid was assumed to be reached when the pH-probe approached stable values. Then, the electrochemical system was allowed to reach steady state. This was assumed to be established when the open circuit potential approached a steady value. Then electrochemical measurements started by first doing a cathodic potentiodynamic sweep.

In order to get better control of mass transport a submerged jet impingement setup was used for some of the latter experiments. The nozzle diameter was the same as that of the electrode, i.e. 6 mm in order to mimic the flow regime at a rotating disc electrode, i.e. laminar flow and uniform mass transport to the electrode surface.[13,14] Calibration of the setup using a sample to nozzle distance of 2 cm and a nozzle speed set to 0.65 m/s gave a hydrodynamic constant which made the system comparable to a rotating disc electrode at 400 rpm.

Table 1
Summary of experimental conditions

Experiment ID	pH	Temp. [°C]	$p(N_2)$ [atm]	p(H2S) [atm]
1	3.8	30	0	1
2	5.0	30	0	1
3	5.9	30	0	1
4	2.1	30	1	0
5	2.1*	45	1	0
6	2.1*	60	1	0
7	4.9	30	0	0.002
8	4.8	30	0	0.12
9	3.9	30	0	1
10	3.9*	45	0	1
11	3.9*	55	0	1
12	2.0	30	1	0
13	3.0	30	1	0
14	4.3	30	1	0

* pH was measured with a calibrated probe at the lower temperature and assumed not to change upon increasing the temperature, an assumption supported by calculations.

RESULTS AND DISCUSSION

The first part of this section presents results and observations from mackinawite synthesis and electrode fabrication, also including some points for future improvements. In the second part we present potentiodynamic sweeps for mackinawite electrodes under different conditions.

‡ Trade name

Mackinawite synthesis and electrode fabrication

X-ray diffractograms, shown in Figure 1, for the powders obtained from our synthesis show mackinawite as the major product. Some NaCl are also present, it probably precipitated in the drying stage and was not removed by rinsing in isopropanol. Also, some weak reflections attributed to greigite are apparent. As indicated in the introductory section mackinawite may transform into greigite in anoxic waters.[6] The intensity of its reflections are, however, so small that we the greigite fraction to be negligible, especially since we have no reason to suspect that greigite is particularly electrochemically active.

We also note that increased relative intensity of greigite reflections with time indicate that it slowly forms during storage. Another sample was left for storage exposed to air, and re-examination (not shown) after a couple of months clearly indicated that it had oxidized to form elemental sulphur (S_8) and probably also some amorphous iron (hydr)oxides. Since no sulphur reflections were found in Figure 1 we rule out oxygen ingress. Transformation of completely dry mackinawite to greigite seems unlikely (it would require $2Fe^{2+} \rightarrow Fe + Fe^{3+}$) and we therefore believe that some moisture was entrapped within the sample holder upon assembly, probably from insufficient drying of the powder. At any rate, mackinawite is essentially the only iron containing phase present in the sample – even after over a year of storage.

Figure 2a shows a SEM-image of powders obtained from mackinawite synthesis. Particles appear to form micron-sized agglomerates, while the primary particle size is somewhat smaller. Our product resemble the irregularly shaped micrometer sized particles produced in another lab by reacting sulfide ions with metallic iron.[15] Flake-like mackinawite crystals are also reported in the literature.[9] Note that the larger octahedral crystals in Figure 2a are NaCl and not iron sulfide. NaCl may crystallize into both cubic and octahedral crystals, with the cubic form being thermodynamically more stable and therefore more common.[16]

A SEM-image of (part of) a polished mackinawite electrode is shown in Figure 2b. Some darker spots (better visible at higher magnification, cf. the insert) are scattered across the entire electrode surface. They represent micrometer-sized voids in the electrode surface and most probably originate from the loss of small NaCl crystals during polishing or during subsequent ultra-sonication in isopropanol. This will introduce surface roughness (or surface porosity) beyond what is expected for a 0.05 µm alumina finish. In future synthesis the amount of NaCl should be reduced by using less NaCl in the solution during synthesis and/or by washing away more salt after the synthesis.

Nevertheless, the mackinawite electrodes appear suitable for use as working electrodes to study the electrochemical properties of mackinawite. The electrical resistance through a polished and epoxy-casted electrode is typically a couple of ohms, similar to the value measured if the mackinawite pellet is replaced with steel. This indicates that the conductivity through the pellet itself is good, and that most of the resistance is probably related to the back contact. The biggest challenge with the electrodes is the mechanical integrity. Before operation the electrodes have surprisingly good mechanical stability, allowing them to be polished essentially to a mirror finish. Also during mild operation in solution the integrity is good. The problem arises when an electrode is polarized far into the cathodic region where significant gas evolution takes place. This gives increased pressure in cracks and pores and eventually rupture and disintegration of the pellet.

Finally, a few points deserve attention regarding synthesis and handling mackinawite. Oxygen must be kept away in order to avoid oxidation. Also, high temperatures should be avoided. In the absence of oxidation, the solid state (dry) transformation from mackinawite to greigite is reported to take place above 180 °C while the rapid transformation from mackinawite to pyrrhotite takes place above 250 °C.[17] This rules out heat treatment (such as high temperature sintering or intermediate temperature necking) in the process of turning powders into an electrode. High pressure was used to obtain a mechanically stable pellet in this work, but one should consider of the possibility of phase transitions if a too high pressure is used. Pressure induced phase transitions have been demonstrated for other iron sulfide polymorphs.[18] Also, the use of a binder may improve the mechanical integrity of the electrode, but care must be taken not to increase the resistance too much.

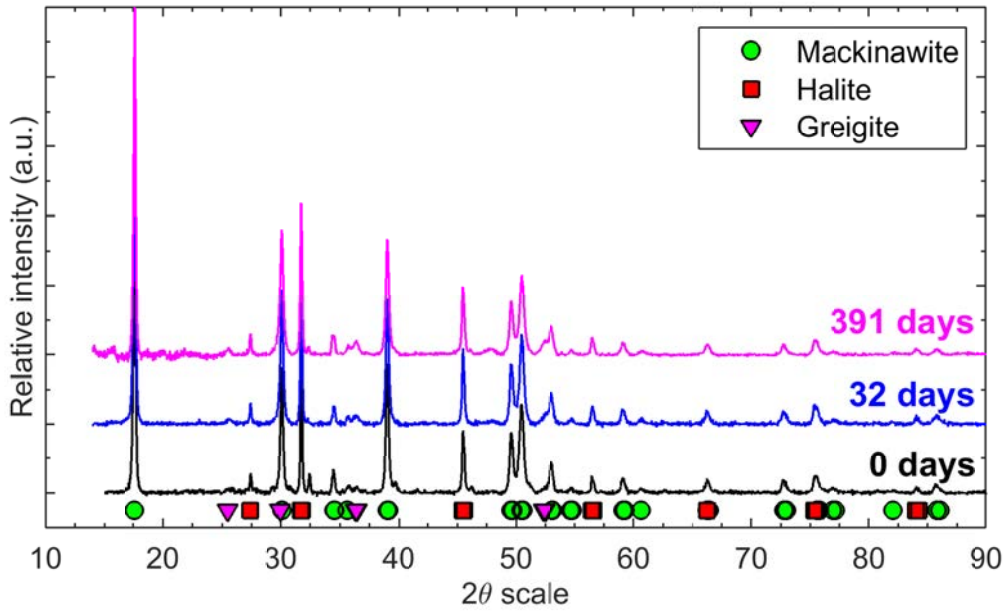

Figure 1: X-ray diffractograms of the products of mackinawite synthesis as a function of storage time. Solid markers in the lower part of the figure mark main reflections from identified phases, indicated in the legend.

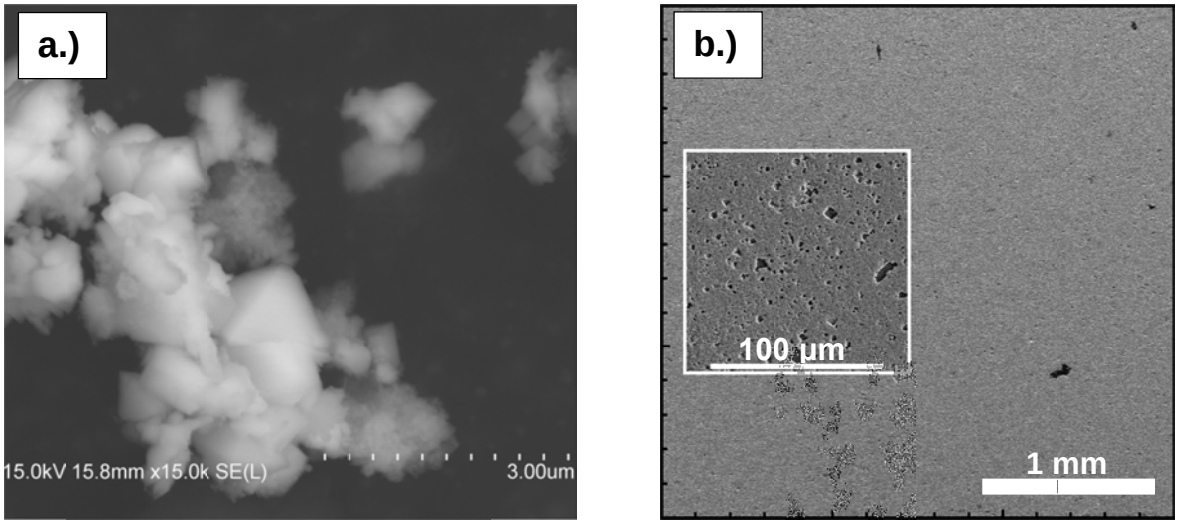

Figure 2: SEM-images of a.) powders produced by mackinawite synthesis and b.) part of a polished mackinawite electrode. The insert shows a zoomed region.

Electrochemical behavior of mackinawite electrodes

In this work all currents have been converted to current densities using the geometrical electrode area (i.e. 0.283 cm^2). As described in the previous section the electrodes have some surface porosity and therefore the current densities may be somewhat overestimated. Methods for determining the electrochemically active surface area using voltammetric charge do exist,[19] and can be routinely used for well-defined electrodes and electrode reactions, but has not been implemented in this work. Potentials are corrected for IR-drop based on resistance values obtained from EIS measurements. All the polarization curves are plotted with the same axis limits to allow direct visual comparison between the figures.

Figure 3 shows potentiodynamic sweeps for a mackinawite electrode under 1 atm N_2 as a function of pH. This set of experiments was done with a nozzle speed of 0.65 $m \cdot s^{-1}$, giving a flow regime corresponding to a rotating disc electrode at 400 rpm. In the cathodic potential range we observe limiting currents at pH 2 and at pH 3 which are just short of one decade apart (strictly speaking the currents differ by a factor 7 at -900 mV vs. the reference). These currents are attributed to mass transport limited proton reduction, and are in in fair agreement with what one would predict from theory. At pH 4.3 any limiting current is obscured by the apparent overlap with a background current.

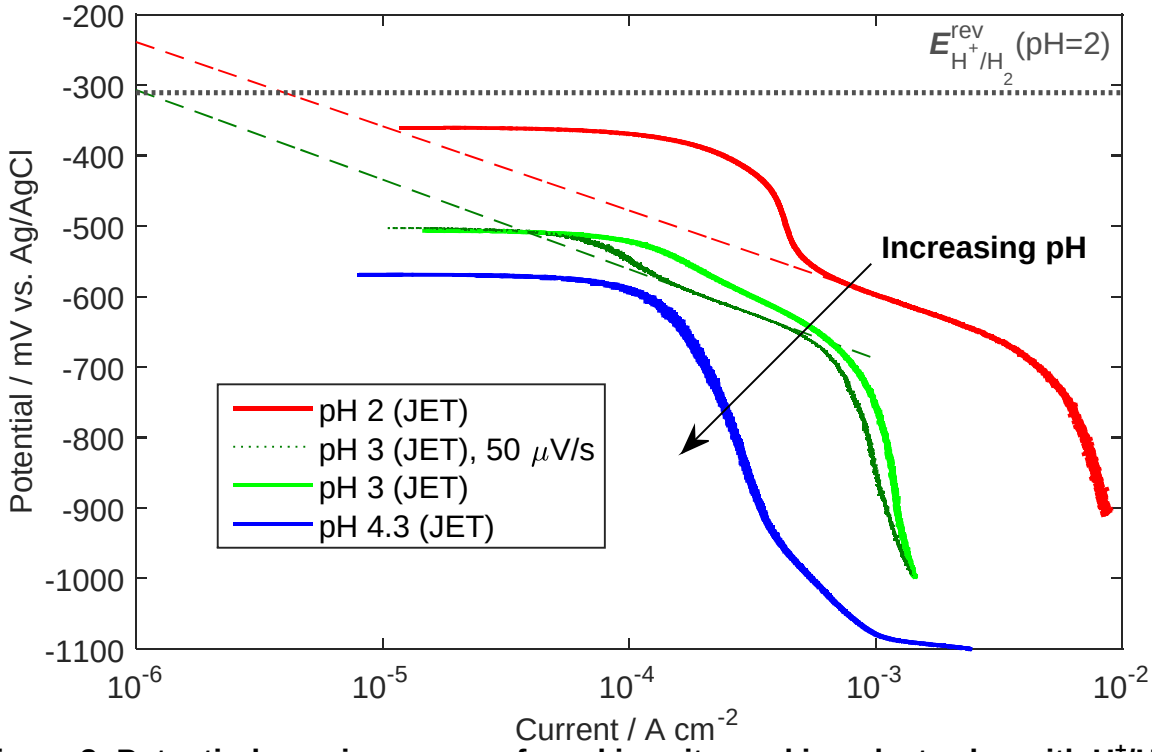

Figure 3: Potentiodynamic sweeps of mackinawite working electrodes with H^+/H_2O as the only oxidant. Experiments were done in a JET-impingement cell with a nozzle speed of 0.65 m/s. The dotted line represents the reversible potential for the hydrogen evolution reaction at pH 2. The dashed lines are Tafel fits obtained by linear regression.

Thus, in order to obtain any reliable kinetic parameters for the hydrogen evolution reaction at mackinawite electrodes we have to look at the experiments with a sufficient proton activity. We fitted experimental data from the linear Tafel-like region (-600 to -640 mV) of the experiment recorded at pH 2 to a Tafel expression of the form

$$i = i_0 \cdot 10^{-\left(E - E^{rev}\right)/b} \quad (1)$$

where i is the current density, i_0 is the exchange current density, E is the potential, E^{rev} is the reversible potential for hydrogen evolution and b is the slope of the linear region. With the potential in mV the resulting expression at pH 2 is

$$i = 4.02 \cdot 10^{-6} \cdot 10^{-(E+314)/120}\ \mathrm{A \cdot cm^{-2}} \quad (2)$$

A Tafel slope of 120 mV/decade agree well with both experimental and theoretical values for steel.[20] If we try to fit the apparently linear region from the pH 3 experiment we get a slope of 169 mV·decade^{-1}. The current in this region, however, appears to be a sum of overlapping currents. Actually, fit to a dataset recorded at a sweep rate of 0.05 mV·s^{-1} (green dotted line in the figure) resulted in better deconvolution so that a slope of 127 mV·decade^{-1} and an exchange current density of $3.10 \cdot 10^{-6}$ A·cm^{-2} was obtained. This, however, still seems to be a region of overlapping currents. We therefore believe that 120 mV·decade^{-1} is the value that best represents proton reduction at mackinawite electrodes for all pH values. The dataset at pH 4.3 has no region that unambiguously represents proton reduction. Around -950 mV, however, there is a narrow linear region that we believe represents water reduction. A significant increase in the current around -1100 mV is assumed to be due to breakdown of the electrode due to water reduction and gas evolution in cracks and pores. At any rate, water reduction is expected to contribute very little to the total current for most practical experimental conditions and have not been investigated further. Future experiments should include measures to increase the region of activation controlled currents by increasing the jet flow rate and/or by using a buffer.

Figure 4 show potentiodynamic sweeps for a mackinawite working electrode in the presence of 1 atm H_2S at different pH. In the intermediate potential range there is an increase in the cathodic currents with decreasing pH, while the currents seem to approach the same values at the far cathodic end. Below say -950 mV the current is most likely entirely governed by reduction of H_2S but the curvature of the plots in this region leads us to believe that mass transport is starting to limit the current. In order to clarify this, future work should include repeating this experiment using forced convection (cf. jet impingement).

Tafel fits to the datasets for pH 5 and pH 5.9 give slopes of 161 and 132 mV·decade^{-1}, respectively. The corresponding exchange current densities are $4.91 \cdot 10^{-6}$ and $2.08 \cdot 10^{-6}$ A·cm^{-2}. Remember that the parameters are referred to the reversible potential according to Eq. (1) and hence also to the pH for that particular experiment. As discussed for the proton reduction data above, also these data appear to lack a clear liner Tafel region – especially for the lower pH values. This could be due to overlapping processes of typically proton reduction and H_2S reduction. If this is the case, then the experiment with the lowest proton activity (i.e. the high pH experiment) will best represent H_2S reduction and the true value is probably close to 132 mV·decade^{-1}. Interestingly this is very close to the 135 mV·decade^{-1} obtained for stainless steel.[20] Kinetic parameters are summarized in Table 2.

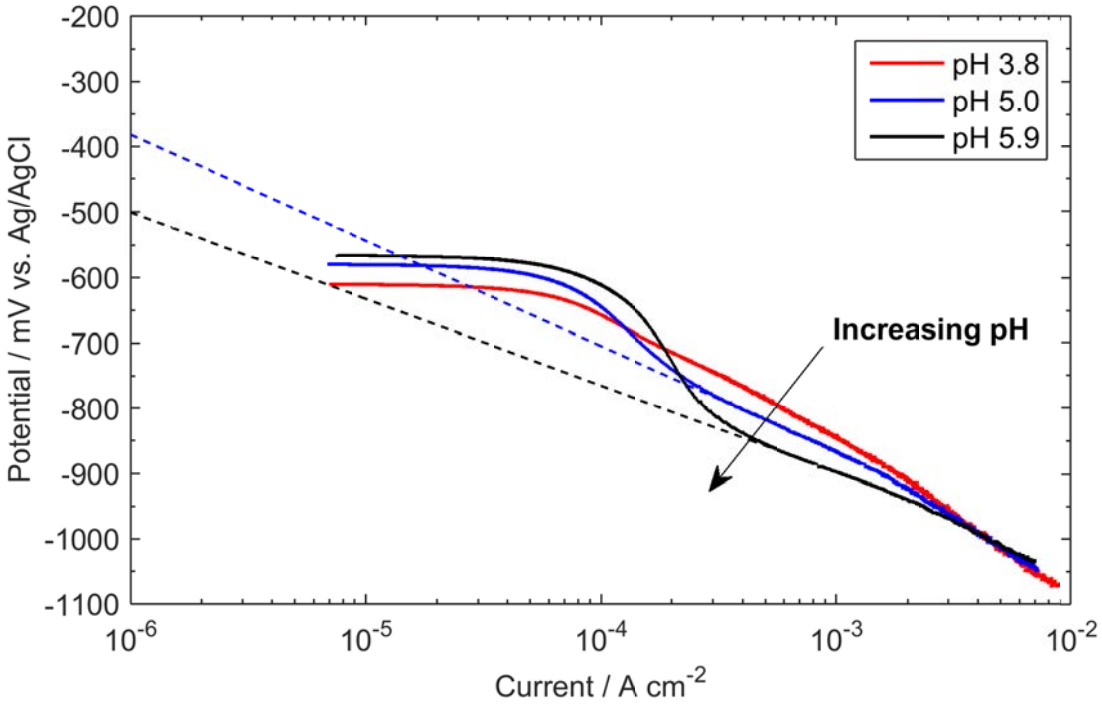

Figure 4: Potentiodynamic sweeps of mackinawite working electrodes in the presence of 1 atm H_2S as a function of pH as indicated in the legend. Experiments were done in a cell with magnetic stirring. The dashed lines are Tafel fits obtained by linear regression.

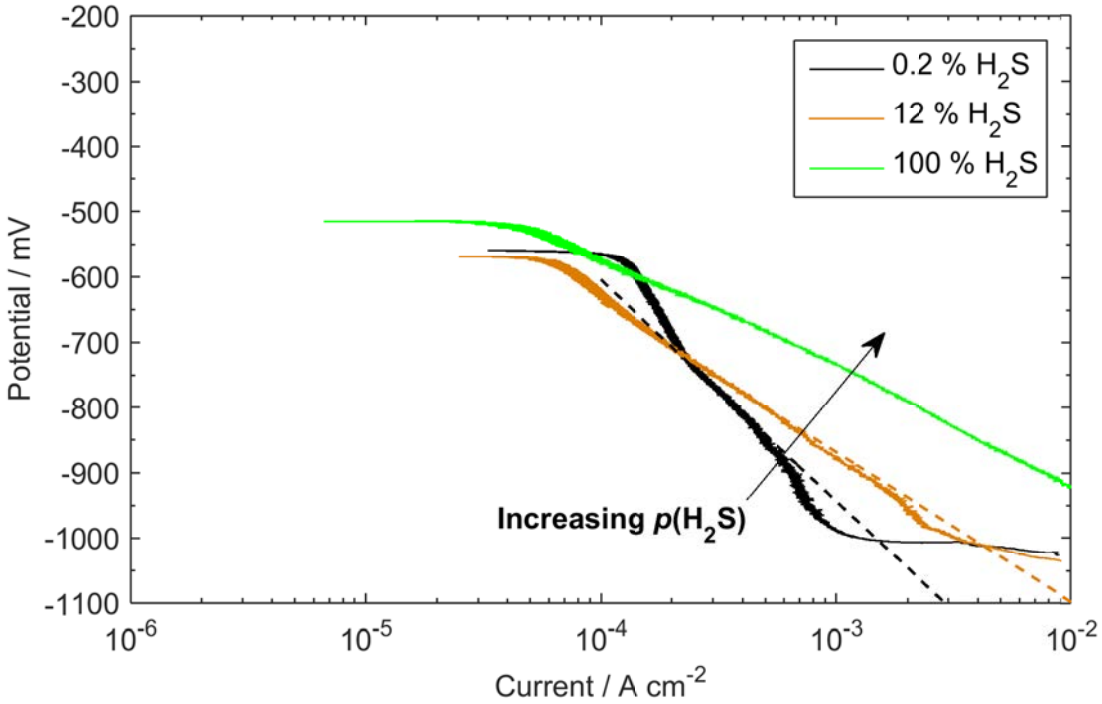

Figure 5: Potentiodynamic sweeps of mackinawite working electrodes as a function of the partial pressure of H_2S as indicated in the legend. The system was not buffered, meaning that pH varied with $p(H_2S)$. Experiments were done in a cell with magnetic stirring.

Figure 5 show potentiodynamic sweeps for a mackinawite working electrode as a function of the partial pressure of H_2S. Note that these experiments were unbuffered, so that pH decreased from approximately 5 to 4 upon going from 0.2 to 100 % H_2S. The increase in current with increasing H_2S concentration is higher than what one would expect from a simple pH effect at this part of the pH range (cf. Figure 3). This strongly supports that direct reduction of H_2S takes place at mackinawite, as it is believed to do at steel.[20] Apparently overlapping currents (i.e. no Tafel region) makes it difficult to obtain the reaction order with respect to H_2S from the current data. Future experiments should include forced convection to help in this matter.

As a first attempt to obtain the temperature dependence of the reactions under study we have performed some experiments at different temperatures. Note that in these series pH was only measured at the lower temperature (30 °C). The pH was then calculated to not vary significantly with temperature, and is thus assumed to be constant.

Figure 6 shows potentiodynamic sweeps of mackinawite working electrodes with H^+/H_2O as the only added oxidant as a function of temperature. The open circuit potential appears to decrease with increasing temperature, but this could also be a time-effect. Short linear-like regions in the potential region around -700 mV are interpreted as kinetically controlled proton reduction. They appear to be essentially unaffected by temperature, but a trend can be seen from the fits (dashed lines in the figure). Kinetic parameters obtained from linear regression are summarized in Table 2.

Figure 7 shows potentiodynamic sweeps of mackinawite working electrodes in the presence of 1 atm H_2S for different temperatures. Here both open circuit potential and current densities increase with increasing temperature. The pH used here (around 4) is not the best to obtain kinetic parameters for H_2S reduction, and any fit will be somewhat ambiguous and depend on the selected fit range. Anyway, the result of the Tafel fits are included as dashed lines in the figure and the corresponding parameters are included in Table 2.

In an attempt to obtain temperature dependence through activation energies we fit the obtained exchange current densities to an Arrhenius type relation

$$i_0 = A \exp\left(-\frac{E_a}{RT}\right) \tag{3}$$

where A is a pre-exponential factor and E_a is the activation energy to be found. Plotting $\ln(i_0)$ against $1/T$, as shown in Figure 8, the activation energy can easily be obtained. For proton reduction, where there was only a small change with temperature, the activation energy is 11 $kJ \cdot mol^{-1}$. This is much lower than the value of 30 $kJ \cdot mol^{-1}$ commonly used for steel electrodes.[3]

Doing the same exercise for the data for H_2S reduction, cf. Figure 8, we obtain an activation energy of 60 $kJ \cdot mol^{-1}$. Interestingly this is exactly the value found for steel.[3] Both these series of experiments should be repeated with forced convection in order to obtain better kinetic data.

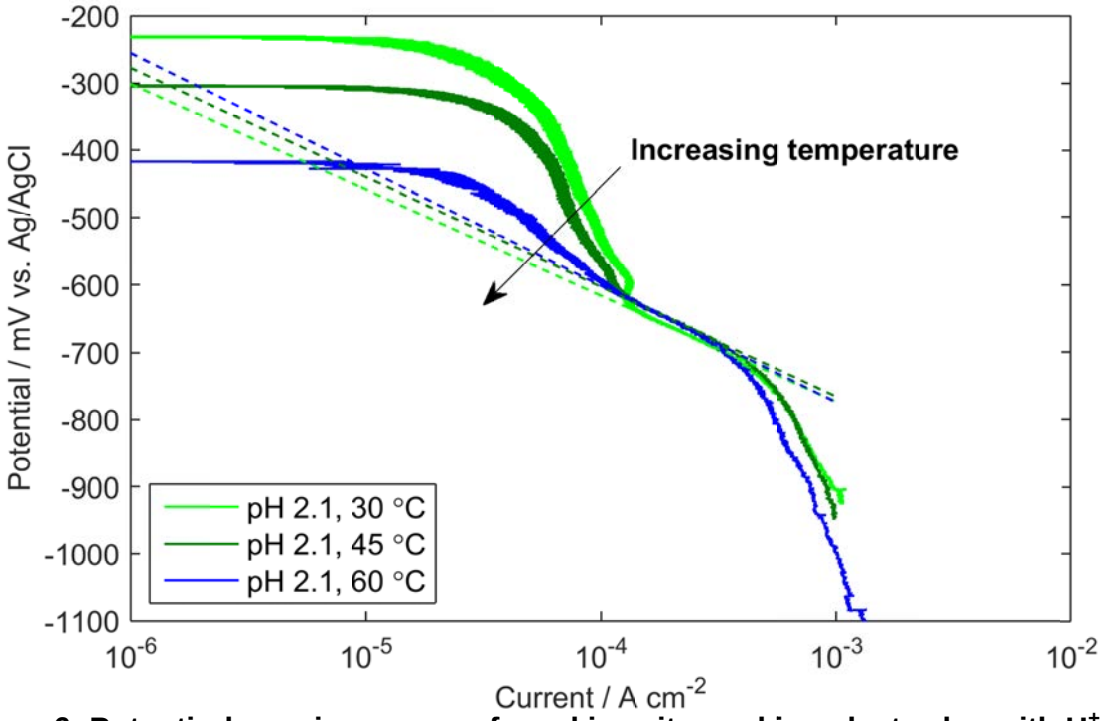

Figure 6: Potentiodynamic sweeps of mackinawite working electrodes with H^+/H_2O as the only added oxidant as a function of temperature. Experiments were done in a cell with magnetic stirring. Dashed lines are Tafel fits from by linear regression.

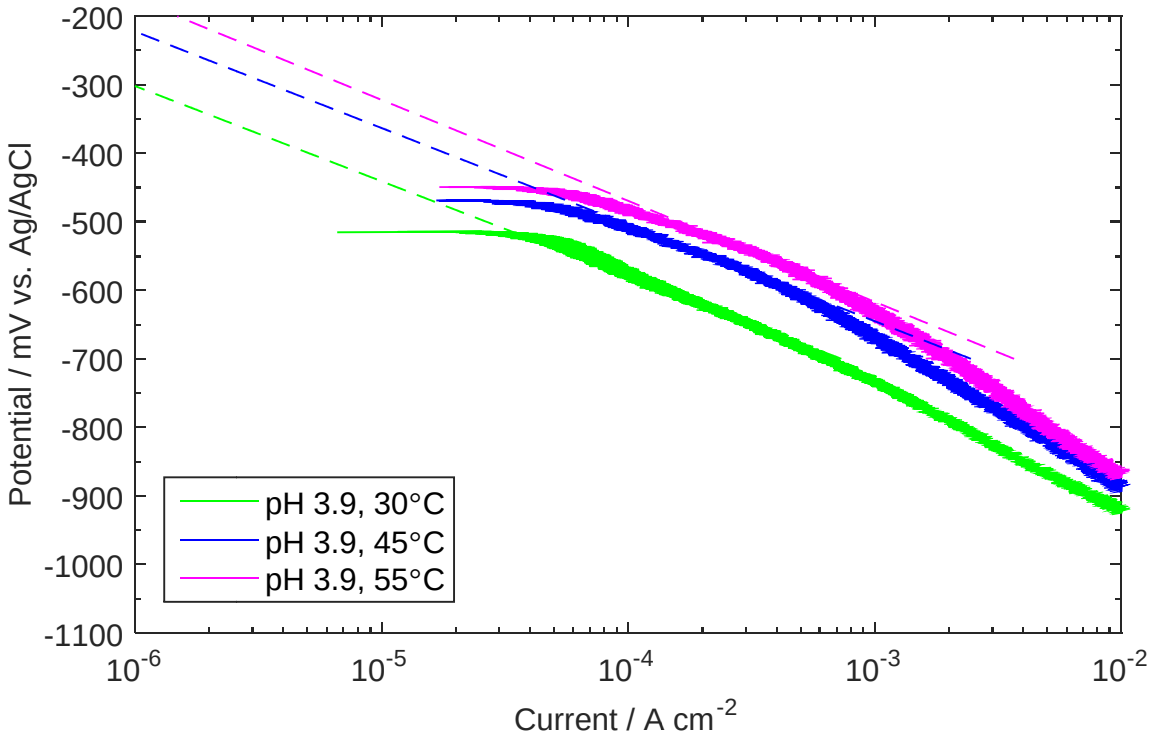

Figure 7: Potentiodynamic sweeps of mackinawite working electrodes in the presence of 1 atm H_2S for different temperatures. Experiments were done in a cell with magnetic stirring.

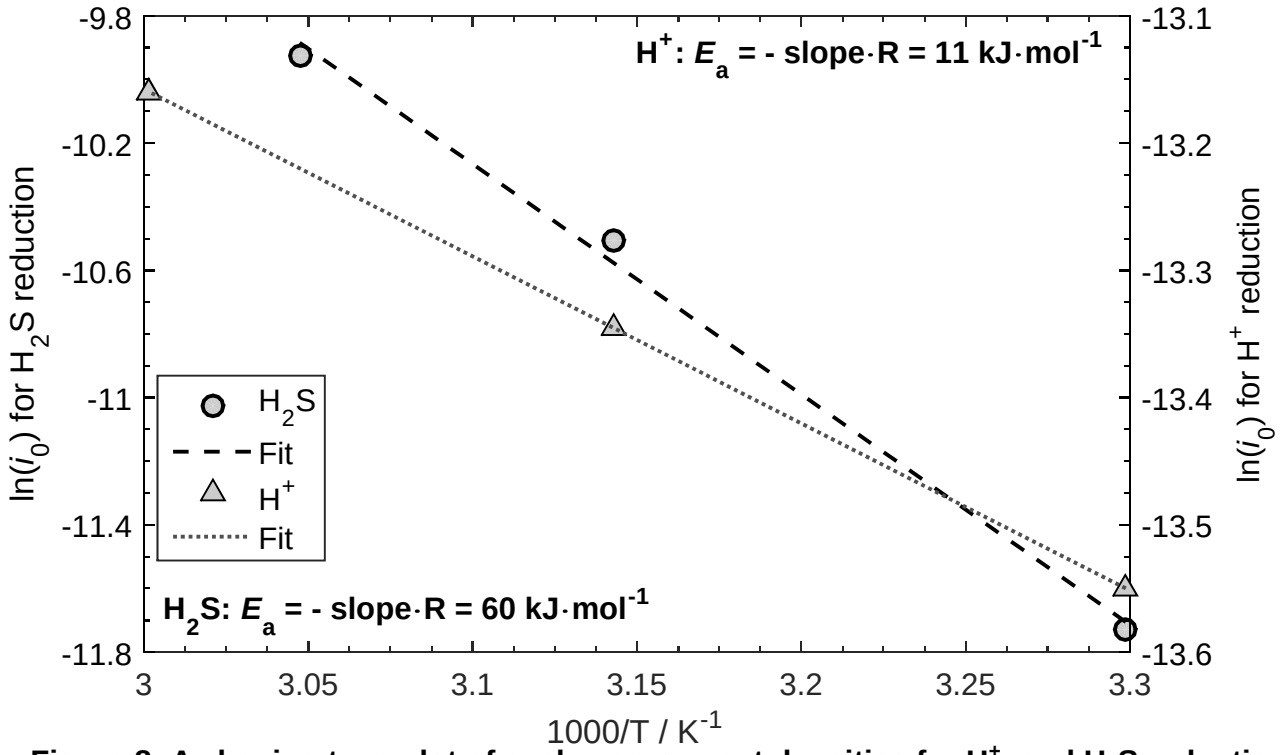

Figure 8: Arrhenius-type plot of exchange current densities for H^+- and H_2S reduction

Table 2
Summary of kinetic parameters obtained from linear regression

Exp. ID	pH	Temp. [°C]	$p(N_2)$ [atm]	$p(H_2S)$ [atm]	Reaction	i_0 [A·cm^{-2}]	b [mV·dec^{-1}]
2	5.0	30	0	1	H_2S/H_2	$4.91 \cdot 10^{-6}$	-161
3	**5.9**	**30**	**0**	**1**	**H_2S/H_2**	**$2.08 \cdot 10^{-6}$**	**-132**
4	2.1	30	1	0	H^+/H_2	$1.30 \cdot 10^{-6}$	-157
5	2.1*	45	1	0	H^+/H_2	$1.61 \cdot 10^{-6}$	-162
6	2.1*	60	1	0	H^+/H_2	$1.92 \cdot 10^{-6}$	-173
9	3.9	30	0	1	H_2S/H_2	$8.03 \cdot 10^{-6}$	-139
10	3.9*	45	0	1	H_2S/H_2	$2.73 \cdot 10^{-5}$	-141
11	3.9*	55	0	1	H_2S/H_2	$4.88 \cdot 10^{-5}$	-147
12	**2.0**	**30**	**1**	**0**	**H^+/H_2**	**$4.02 \cdot 10^{-6}$**	**-120**
13	3.0	30	1	0	H^+/H_2	$3.10 \cdot 10^{-6}$	-127

* pH was measured with a calibrated probe at the lower temperature and assumed not to change upon increasing the temperature, an assumption supported by calculations.

In order to study single electrode reactions and obtain parameters needed for the construction of current-potential relations one has to look at different ranges of conditions. Proton reduction is best studied at low pH in the absence of other oxidants. Reduction of H_2S is best studied in a solution saturated with H_2S at a relatively high pH where the proton concentration is too low for its reduction to contribute significantly to the cathodic current. In light of this we believe that the data obtained from experiment 3 and experiment 12 give the most reliable kinetic

parameters. Data from the other experiments should be re-visited, and preferably be compared to similar experiments with forced convection.

It is worth noting that extreme pH values may introduce other complications. A very low pH increases the solubility of iron sulfides to impractically high values, and very high pH values favor precipitation of iron (hydr)oxides, carbonates and sulfides. This calls for a compromise in the choice of experimental conditions, and this was the reason for selecting pH 2 as the lower limit and pH 6 as the higher limit in this work.

In the intermediate pH range (around pH 4) both proton reduction and H_2S reduction takes place at iron sulfide electrodes during cathodic polarization. Considering the thermodynamic equivalence of the two reactions [3] it is not surprising that both reactions take place at the same potentials. We could not find any literature on mackinawite electrodes to compare our results with. Still, it is interesting to compare the kinetic parameters to those available for steel to see which is more active towards the cathodic reactions. As mentioned above, Tafel slopes obtained for mackinawite in this work are similar to available values for steel electrodes.

Comparing exchange current densities (or current densities at the equilibrium potential) is not as straight forward due their concentration dependence and the different conditions used in different reports. A way to overcome this is to use refer everything to a set of standard conditions and to include a term taking into account the concentration variation. Unfortunately, the limited data available for mackinawite electrodes has made it difficult to obtain consistent reaction orders and this has not been included in the kinetic expressions as of yet. What we can do, however, is to compare data to experiments at steel electrodes performed at similar conditions.

Such a comparison is possible for proton reduction at pH 3 from Figure 2 in the publication by Zheng *et al*.[20] Here we read the current density at -400 mV vs. Ag/AgCl as $8 \cdot 10^{-6}$ $A \cdot cm^{-2}$. This is very close to the $5 \cdot 10^{-6}$ $A \cdot cm^{-2}$ obtained from Figure 3 in this work. We would therefore say that the two materials appear to be essentially equally active towards proton reduction (at least at pH 3). For H_2S reduction, such a comparison is not currently available.

CONCLUSIONS

A method for producing mackinawite electrodes has been developed. The electrodes seemed to be applicable for the study of electrochemical properties of mackinawite, but experienced some mechanical problems when significant gas evolution took place. Future work should include efforts to improve the mechanical integrity of electrodes.

From the kinetic data obtained in this work it appears that mackinawite has similar activity as steel when it comes to reduction of protons and for H_2S. Actually, many kinetic parameters are essentially identical to literature values for steel electrodes. Experiments allowing determination of reaction orders for protons and H_2S should be included in future work.

This suggests that possible galvanic effects are expected to be small between equally sized electrodes. There is, however, the possibility of having significant area ratio with a high surface area porous iron sulfide deposit layer on a steel substrate. In such a situation the galvanic effect may become severe and contribute to unacceptable corrosion rates.

ACKNOWLEDGEMENTS

The authors acknowledge The Research Council of Norway (contract no. 228222) and the industrial partners in the project (Baker Hughes, BG Group, Clariant, ConocoPhillips, ExxonMobil, Nalco Champion, Shell and Total) for funding.

REFERENCES

1. M. Bonis, M. Girgis, K. Goerz, R. MacDonald, Weight Loss Corrosion with H2S: Using Past Operations for Designing Future Facilities, in: 61st Annual Conference & Exposition, Corrosion 2006, NACE, 2006.

2. S. Nesic, S. Wang, H. Fang, W. Sun, J.K.-L. Lee, A New Updated Model of CO2/H2S Corrosion in Multiphase Flow, in: Corrosion 2008, NACE, 2008.

3. Y. Zheng, B. Brown, S. Nešić, Electrochemical Study and Modeling of H2S Corrosion of Mild Steel, Corrosion, 70 (2013) 351-365.

4. C.M. Menendez, V. Jovancicevic, S. Ramachandran, M. Morton, D. Stegmann, Assessment of Corrosion Under Iron Sulfide Deposits and CO2/H2S Conditions, Corrosion, 69 (2012) 145-156.

5. J. Kvarekvål, G. Svenningsen, Effect of Iron Sulfide Deposits on Sour Corrosion of Carbon Steel, in: Corrosion/2016, NACE International, 2016, pp. 7478.

6. D. Rickard, G.W. Luther, Chemistry of Iron Sulfides, Chemical Reviews, 107 (2007) 514-562.

7. J. Ning, Y. Zheng, D. Young, B. Brown, S. Nešić, Thermodynamic Study of Hydrogen Sulfide Corrosion of Mild Steel, Corrosion, 70 (2013) 375-389.

8. M. Tjelta, J. Kvarekvål, Electrochemistry of Iron Sulfide and its Galvanic Coupling to Carbon Steel in Sour Aqueous Solutions, in: Corrosion/2016, NACE International, 2016, pp. 7478.

9. F. Shi, L. Zhang, J. Yang, M. Lu, J. Ding, H. Li, Polymorphous FeS corrosion products of pipeline steel under highly sour conditions, Corrosion Science, 102 (2016) 103-113.

10. S.N. Smith, M.W. Joosten, Corrosion of Carbon Steel by H2S in CO2 Containing Oilfield Environments - 10 Year Update, in: Corrosion/2015, NACE International, 2015, pp. 5484.

11. M. Tjelta, J. Kvarekval, Electrochemical properties of iron sulphide in weak acid systems, in: EUROCORR 2014, Pisa, 2014.

12. M. Tjelta, J. Kvarekval, Electrochemistry of iron sulphides in sour aqueous solutions, in: EUROCORR 2015, Graz, 2015.

13. J.M. Esteban, G.S. Hickey, M.E. Orazem, The Impinging Jet Electrode: Measurement of the Hydrodynamic Constant and Its Use for Evaluating Film Persistency, Corrosion, 46 (1990) 896-901.

14. E. Gulbrandsen, A. Granå, Testing of Carbon Dioxide Corrosion Inhibitor Performance at High Flow Velocities in Jet Impingement Geometry. Effects of Mass Transfer and Flow Forces, CORROSION, 63 (2007) 1009-1020.

15. M. Mullet, S. Boursiquot, M. Abdelmoula, J.-M. Génin, J.-J. Ehrhardt, Surface chemistry and structural properties of mackinawite prepared by reaction of sulfide ions with metallic iron, Geochimica et Cosmochimica Acta, 66 (2002) 829-836.

16. P.E. Smith, The effect of urea on the morphology of NaCl crystals: A combined theoretical and simulation study, Fluid phase equilibria, 290 (2010) 36-42.

17. A.R. Lennie, K.E.R. England, D.J. Vaughan, Transformation of synthetic mackinawite to hexagonal pyrrhotite; a kinetic study, American Mineralogist, 80 (1995) 960-967.

18. K. Kusaba, Y. Syono, T. Kikegawa, O. Shimomura, Structures and Phase Equilibria of FeS Under High Pressure and Temperature, in: Properties of Earth and Planetary Materials at High Pressure and Temperature, American Geophysical Union, 2013, pp. 297-305.

19. S. Ardizzone, G. Fregonara, S. Trasatti, "Inner" and "outer" active surface of RuO2 electrodes, Electrochimica Acta, 35 (1990) 263-267.

20. Y. Zheng, J. Ning, B. Brown, S. Nesic, Investigation of Cathodic Reaction Mechanisms of H2S Corrosion Using a Passive SS304 Rotating Cylinder Electrode, in: Corrosion/2016, NACE International, 2016, pp. 7340.